Journal of Asian Ceramic Societies

ISSN: (Print) 2187-0764 (Online) Journal homepage: https://www.tandfonline.com/loi/tace20

Preparation and characterization of hydroxyapatite from *Achatina achatina* snail shells: effect of carbonate substitution and trace elements on defluoridation of water

Bernard Owusu Asimeng, Joseph Richmond Fianko, Elsie Effah Kaufmann, Elvis Kwason Tiburu, Claude Fiifi Hayford, Prince Atsu Anani & Obed Korshie Dzikunu

To cite this article: Bernard Owusu Asimeng, Joseph Richmond Fianko, Elsie Effah Kaufmann, Elvis Kwason Tiburu, Claude Fiifi Hayford, Prince Atsu Anani & Obed Korshie Dzikunu (2018) Preparation and characterization of hydroxyapatite from *Achatina achatina* snail shells: effect of carbonate substitution and trace elements on defluoridation of water, Journal of Asian Ceramic Societies, 6:3, 205-212, DOI: 10.1080/21870764.2018.1488570

To link to this article: https://doi.org/10.1080/21870764.2018.1488570

Accepted author version posted online: 21 Jun 2018.
Published online: 20 Jul 2018.

JOURNAL OF ASIAN CERAMIC SOCIETIES
2018, VOL. 6, NO. 3, 205–212
https://doi.org/10.1080/21870764.2018.1488570

THE CERAMIC SOCIETY OF JAPAN
THE KOREAN CERAMIC SOCIETY
Taylor & Francis
Taylor & Francis Group

FULL LENGTH ARTICLE

OPEN ACCESS Check for updates

Preparation and characterization of hydroxyapatite from *Achatina achatina* snail shells: effect of carbonate substitution and trace elements on defluoridation of water

Bernard Owusu Asimeng [a], Joseph Richmond Fianko[b], Elsie Effah Kaufmann [a], Elvis Kwason Tiburu[a], Claude Fiifi Hayford [a], Prince Atsu Anani [a] and Obed Korshie Dzikunu [a]

[a]Department of Biomedical Engineering, University of Ghana,Legon, Ghana; [b]Department of Nuclear Sciences and Applications, Ghana Atomic Energy Commission, Accra Ghana

ABSTRACT

A novel hydroxyapatite [HAp: $Ca_{10}(PO_4)_6(OH)_2$] material for defluoridation was prepared from *Achatina achatina* (AA) snail shells using a modified chemical precipitation method. X-ray diffractometry and atomic absorption spectrometry revealed carbonate substitution as a function of stirring conditions. Stirring time was varied to control crystallite size and trace element concentrations. In addition, Infrared spectra, cyclic voltammograms, and ion exchange profiles confirmed the functional groups, the surface mass concentration and the fluoride removal efficiency, respectively. It was observed that the samples prepared after 1 hr optimal stirring times reduced fluoride concentration from 20.00 to $1.59 \pm 0.06 mgL^{-1}$ without affecting the overall pH conditions of the water, whereas beyond this time frame, low uptake of the fluoride ions was obtained with increasing pH conditions. It was also observed that crystallite size did not affect the removal capacity of the samples. The results demonstrated herein the possibility of using locally prepared AA shells for water purification and other environmental remediation applications.

ARTICLE HISTORY
Received 3 March 2018
Accepted 1 June 2018

KEYWORDS
Hydroxyapatite; carbonates apatite substitution; defluoridation and water purification

1. Introduction

Hydroxyapatite [HAp: $Ca_{10}(PO_4)_6(OH)_2$] is an inorganic material naturally derived from calcium apatite sources such as bones, shells, and corals [1–4]. HAp has been used extensively in various applications including biomedical applications, water purification and other environmental remediation [5–8].

Specifically, in the area of water purification, it has been used to remove fluoride in drinking water using ion exchange and adsorption mechanisms [9,10]. However, the fluoride removal (defluoridation) capacity of HAp has been reported to be low and efforts have been dedicated to identify new and improved methods of defluoridation. This includes preparing the HAp from biogenic sources [9,10] and also by the introduction of nanoparticles into HAp [11,12]. The underlying issue associated with the aforementioned methods of defluoridation is the influence on the pH conditions of the supernatant, which is due to the release of surface ions and/or interstitial ions from the HAp. This requires buffering for correction, thus increasing the cost of defluoridation.

Several attempts have also been made to predict the structural requirements of carbonate substitution in HAp for biomedical applications using theoretical and computational modelling. Thus, three types (Type A, Type B, and Type *AB*) of these substitutions have been simulated [13–16]. In Type A; CO_3^{2-} substitutes the OH^- group in HAp. In Type B; CO_3^{2-} substitutes the PO_4^{3-} group and Na^+ substitutes Ca^{2+} whilst in Type *AB*; PO_4^{3-} and OH^- are substituted by CO_3^{2-}. Whether these predicted substitutions could influence the pH condition of the purified water has not yet been investigated. The substituted ions are expected to form energetic compound and hence will be available for adsorption and not ion exchange. Thus, for effective pH control, we propose to prepare Type B, and/or Type *AB* HAp from *Achatina achatina* (AA) snail shells. The AA snail shells are known to be a good source of calcium carbonate ($CaCO_3$) [17–19] and trace elements including Al, P, K, Ca, Na, Fe, Sr, V, Cd and Pb [20]. This is because the soil in sub-Saharan Africa is made up of these elemental constituents and through the feeding habits of the snails, the ions are ingested which in turn contribute to their shell composition [18,21].

In order to achieve the above objective, HAp was prepared by a chemical precipitation method using calcite from the AA snail shells. Stirring time was varied to control particle size and trace element concentration for HAp charge compensation, after which the samples were characterized using X-ray diffractometer (XRD), Fourier transform infrared spectrometer (FT-IR), atomic absorption spectrometer (AAS), cyclic voltammetry (CV), and defluoridation test performed using ion chromatography (IC).

CONTACT Bernard Owusu Asimeng boasimeng@ug.edu.gh

2. Experimental

2.1. Materials

Snail shells (AA) were collected from snail vendors in Ghana and were identified by the Department of Animal Biology and Conservation Sciences (DABCS) of the University of Ghana.

2.2. Preparation and calcination of the AA shells

The snail shells were washed thoroughly with tap water using a brush and rinsed in distilled water to remove mud and other impurities. After rinsing, they were dried under direct sunlight for 6 hrs. The dried snail shells were then crushed using a mortar and pestle and ground using the Retsch grinder into powder form for calcination. The powder was calcined at 700°C, for 2 hrs to decompose organic material and convert the carbonate into calcite.

2.3. HAp synthesis

HAp samples (n = 5) were synthesized for the study. 5.9 g of diammonium hydrogen phosphate (BDA Lab Suppliers, England) was added to 0.15 cm^3 of distilled water to produce 0.3 M diammonium hydrogen phosphate (DHP) solution of pH 8.12. 5.7 g of calcite was also deposited in 0.15 cm^3 of distilled water while stirring. The DHP solution was then added to the calcite in a drop-wise manner and the resulting solution was stirred using a magnetic stirrer hot plate for 1, 3, 6, 9, and 12 hrs at a constant temperature of 40°*C* for different samples, respectively. These resulting mixtures at stirring time: 1 hr, 3hrs, 6 hrs, 9 hrs, and 12 hrs were labelled as HAp1, HAp3, HAp6, HAp9, and HAp12, respectively and were allowed to age for 24 hrs, thereby allowing atoms to occupy their equilibrium lattice positions in the crystal structure. The precipitates were filtered and dried in an oven at a temperature of 100°C for 2 hrs to produce HAp powders.

2.4. Characterization techniques

The phase compositions of the prepared HAp samples were studied using a PANalytical Empyrean X-ray diffractometer, equipped with Cu Kα radiation (λ = 1.5406 Å). The data were analyzed in the 2θ range of 20–60° with a scan step of 2° per min. The phases were identified by comparing XRD patterns of the HAp powders to the Joint Committee on Powder Diffraction Standards (JCPDS) file using HighScore (Plus) 4.0. The XRD pattern of the HAp samples has many peaks at a range of about 7–90°. However, literature reveals that most of the data required for analysis are collected in the range of 20–60°.The most intense peaks in the range of 30–35° were used to determine the crystallite sizes and the unit cell parameters. crystallite sizes were calculated using Debye-Scherer's equation [22,23] and the unit cell parameters were determined using UnitCell; a least squares refinement program. The hkl indices and their corresponding 2theta positions were used to reclaim unit cell parameters.

FT-IR was used to investigate the functional groups present in the raw AA powders and prepared HAp samples. The spectra were obtained over the region of 400 – 4000 cm^{-1} [24–26]. The scan was conducted using PerkinElmer Spectrum Version 10.03.09.I.

AAS was performed to determine the presence and concentration of trace elements in the prepared HAp samples using a PinAAcle 900 AA Spectrometer which operates at selectable spectral bandwidths of 0.2, 0.7 and 2.0 nm [27]. 10 ml of sulphuric acid and hydrogen peroxide in the ratio (7:3) was added to 1.0 g of dry HAp samples in a 125 ml pyrex conical flask. The resulting solution was heated on a hot plate in a fume hood until it changed color from black to dark brown. The mixture was allowed to cool till it turned colorless. It was then transferred to a 100 ml volumetric flask and topped up with distilled water for characterization.

CV measurement was done to study the concentration of trace elements in the samples and their respective electron transfer interactions. 100 μL of 1 M KCl was added to 15 mg of HAp powders and vortexed for 1 min. A CheapStat potentiostat (IORodeo, USA) with optimized parameters; a start and a stop voltage of −690 mV and 900 mV, respectively, a scan rate of 5mV/sample and a slope of 290 mV/sec was used. Currents were recorded in steps of 50 μA. All measurements were taken using Ag/AgCl Interdigited Electrodes (DropSen, UK).

2.5. Fluoride removal test and pH measurement

20 mgL^{-1} of fluoride solution was prepared by dissolving NaF in distilled water. 15 mg of each HAp powder sample was weighed into 1.15 ml of the prepared fluoride solution. The resulting mixture was agitated for 6 hrs at 125 rpm. The solution was then centrifuged at 1300 rpm for 5 min and 1 ml of the supernatant of each solution pipetted into eppendorf tubes for IC and pH measurement, and the samples were analyzed in triplicate.

Dionex ICS-90 IC was used to determine the concentration of the fluoride (F^-). The IC is controlled by Chromeleon chromatography software v. 6.8 and Peak nitrogen generator. The IC performs isocratic ion analyses using suppressed conductivity detector, liquid eluent, a high-pressure pump, a sample injector AS14A-5μm separator column, AG14A guard column, and Anion microMembrane Suppressor (AMMA 111).

Supernatants were filtered using Sartorius polycarbonate filtering and 0.45 μm cellulose acetate membrane filters after which 20 μL of filtered liquids were injected into an anion exchange column for separation. The separated anions were detected and compared with a calibration curve.

The pH of the supernatant was measured by Mettler Toledo Seven Compact InLab®Expert Pro-DM pH meter.

3. Results and discussion

3.1. XRD analysis

XRD patterns obtained for uncalcined and calcined raw shell powders are presented in Figure 1(a) and (b), respectively. The pattern in Figure 1(a) indicates the presence of aragonite in the uncalcined raw shell powders. Aragonite and calcite are two main crystal forms of calcium carbonate. Aragonite is orthorhombic and forms at low temperatures on the surface of minerals whilst calcite has a trigonal crystal structure which evolves at high temperatures. Calcite is more stable and is insoluble at lower temperatures as compared to aragonite. Hence, it is more widely used in HAp synthesis than aragonite [28]. Figure 1(b) shows aragonite transformation to calcite at 700°C through thermal treatment.

Figure 2 shows the XRD patterns of HAp formed from calcite and DHP solution. HAp1 shows major phases of HAp with minor phases of calcite but HAp3 shows the reverse, major phases of calcite and minor phases of HAp. This is inconsistent with the expectation that calcite ($CaCO_3$) decomposes to CaO and CO_2 and NH_4HPO_4 to NH_4OH and PO_4^{3-} at a constant temperature with increasing stirring time to form HAp.

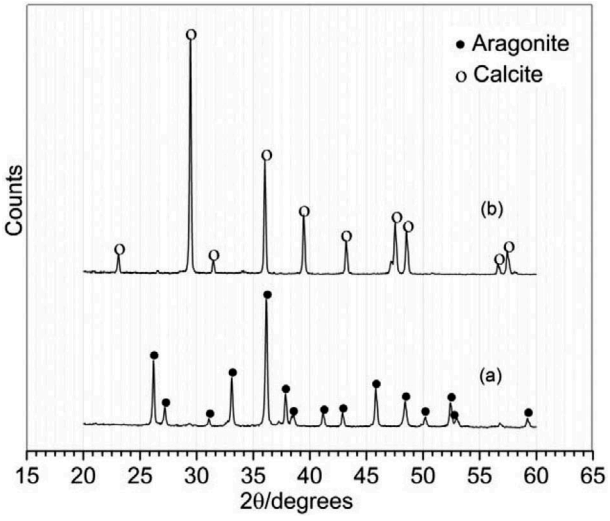

Figure 1. X-ray diffraction patterns of powder from snail shells (a) raw powder (b) calcined powder at 700°C.

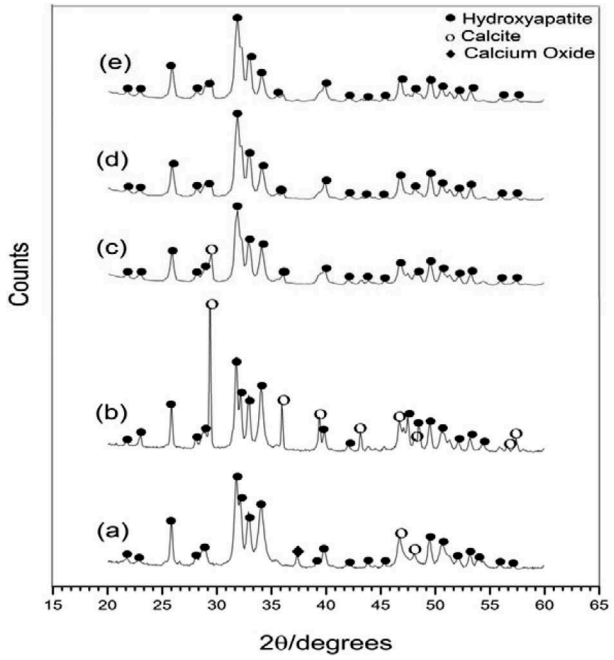

Figure 2. X-ray diffraction patterns of HAp prepared at different stirring times (a) HAp1 (b) HAp3 (c) HAp6 (d) HAp9 (e) HAp12.

From the XRD patterns obtained, full decomposition was not achieved with calcite in HAp3. The absence of the major calcite peaks in HAp1 and its subsequent appearance in HAp3 is suggestive that carbonate groups have been masked by phosphate (PO_4^{3-}) in HAp1. This indicates that CO_3^{2-} has taken one of the six (6) crystal positions of phosphate in the HAp1 structure [29,30]. XRD uses the principle of crystal orientation to identify phases of crystalline materials and hence, once the orientation of a crystal in a material matches a pattern in the XRD database, it is identified as that material.

The calcite phases however subsequently diminished with HAp6 showing fewer calcite major peaks than HAp3. This indicates full decomposition of the carbonate to calcium hydroxide, a precursor of HAp [31]. Pure phase of HAp was revealed by the XRD patterns for HAp9 and that for HAp12 (see Figure 2 (d) and (e)). The unit cell parameters shown in Table 1 indicate an increase in both a and c lattice parameters (0.023 and 0.019, respectively) HAp1 is compared to HAp12. This is associated with a mixed type *AB* carbonate substitution and it is comparable to reported theoretical and experimental simulated results [13]. The XRD patterns of HAp6, HAp9 and

Table 1. Calculated crystallite size and unit cell parameters of the samples.

Sample	Crystallite size/nm	a (Å)	c (Å)
HAp1	30.83	9.43236	6.87785
HAp3	35.72	9.42665	6.87806
HAp6	15.86	9.40923	6.85905
HAp9	15.72	9.40923	6.85905
HAp12	15.52	9.40923	6.85905

HAp12 show broader peak widths than HAp1 and HAp3. This indicates that crystallite sizes of the HAp samples were affected by stirring time. Increasing the stirring time of the calcite and DHP solution produced smaller crystallite size as shown in Table 1.

3.2. Infrared (IR) spectroscopy

Figures 3 and 4 display FT-IR spectra of the uncalcined raw shell powders, calcined shell powders and HAp samples, respectively. The spectra are characterized by two regions; the main region and the fingerprint region on the right side of the graph spanning about 400 cm^{-1} to about 1500 cm^{-1}. The fingerprint region was used to identify the major functional groups of the samples. The spectra in Figure 3(a) and (b) were compared to the Database of ATR-FT-IR spectra of various materials [32]. The matches support the presence of aragonite and calcite, respectively. The major vibration CO_3^{2-} bonds in aragonite and calcite occur at a wavenumber of 1446 cm^{-1} and 1392 cm^{-1}, respectively. Aragonite is normally associated with ores and the 1083 wavenumber corresponds to sulfate.

Figure 4 represents the FT-IR spectra of HAp formed from calcite and DHP. HAp12 shows the presence of phosphate (PO_4^{2-}) bending peaks occurring around the wavenumbers 1089, 1028, 963, 600, 563, and 473 cm^{-1} indicating the presence of HAp.

The principal peaks at 1089 and 1028 cm^{-1} are identified as symmetric $\nu 3$ vibration of the PO_4^{3-} group, while the other two peaks occurring around 963 and 600 cm^{-1} range are due to $\nu 1$ and $\nu 4$ symmetric P–O stretching vibrations of the PO_4^{3-} group, respectively [33]. The OH^- functional group occurring around the wavenumber 634 cm^{-1} in the fingerprint region also confirms the hydroxyl groups of

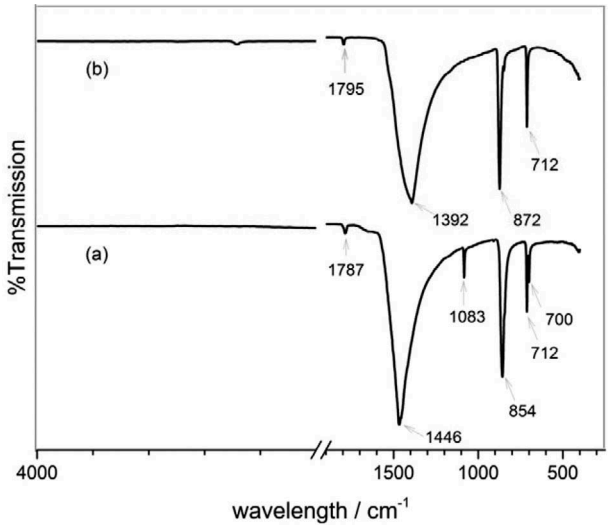

Figure 3. FT-IR spectra of (a) uncalcined raw powder (b) calcined powder at 700°C.

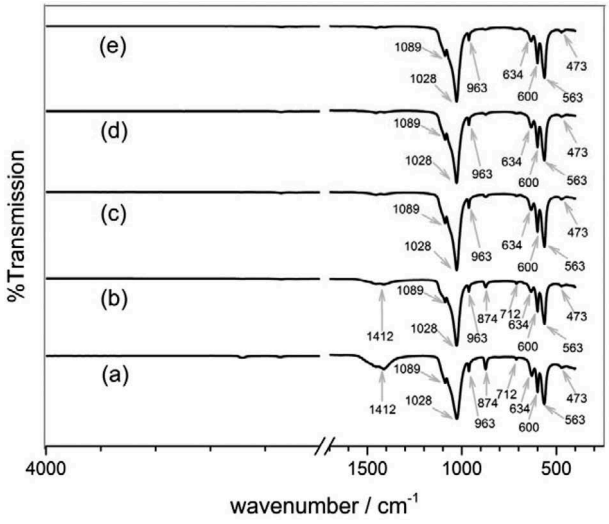

Figure 4. FT-IR spectra of HAp powders prepared at different stirring times (a) HAp1 (b) HAp3 (c) HAp6 (d) HAp9 (e) HAp12.

HAp [34]. The spectra of HAp1 and HAp3 show the presence of CO_3^{2-} around the wavenumbers 1412, 874, and 712 cm^{-1} for both samples. The stretching broad carbonate peaks at band 1412 cm^{-1} indicate that not all the calcites were decomposed or degenerated at 1 and 3 hrs stirring time. This observation is in line with the carbonate-HAp fingerprints reported [35]. The CO_3^{2-} peaks were almost nonexistent; the peaks disappeared for HAp6, HAp9, and HAp12.

The symmetric $\nu 3$ vibration mode of PO_4^{3-} at 1028 cm^{-1} of HAp1 reduced when compared to HAp12 (see Figure 4). The reduction in the transmittance of HAp1 is an indication of a change in the optical depth,τ and this was suspected to be due to carbonate substitution. This observation is consistent with reported IR spectra results on carbonate substitution in HAp [15]. The substitution also affected the liberational OH^- group at wavenumber 634 cm^{-1} and as a result showed a deviation of a path between the $\nu 2$ modes of PO_4^{3-}.

3.3. AAS

Table 2 shows the AAS results of the calcined shell powders and HAp formed at varied stirring times. It is expected that the eating habits of the snails influence the presence of trace elements in the shell. AAS was performed on the HAp samples to detect sodium (Na), iron (Fe), potassium (K), zinc (Zn), copper (Cu), magnesium (Mg), lead (Pb), and cadmium (Cd). The results revealed high concentrations of Na, K and low concentrations of Fe, Zn, Pb, and Cd, whilst Cu and Mg concentration were below detection limit (BDL).Stirring time affected trace element concentration in the HAp samples as shown in Figure 5. A low concentration of Na was obtained for

Table 2. Results showing trace element concentration in $\mu g.L^{-1}$ of HAp samples.

Samples	Na	Fe	K	Zn	Cu	Mg	Pb	Cd
HAp1	0.0732	0.54802	0.009	0.0061	BDL	BDL	< 0.0000001	0.000002
HAp3	0.1765	0.04106	0.013	0.0000	BDL	BDL	0.001212	0.000002
HAp6	0.809	0.04241	0.0368	0.0028	BDL	BDL	0.000699	0.000002
HAp9	1.342	0.05234	0.0409	0.0035	BDL	BDL	< 0.000001	0.000002
HAp12	1.037	0.03669	0.0239	0.0021	BDL	BDL	0.000822	0.000002

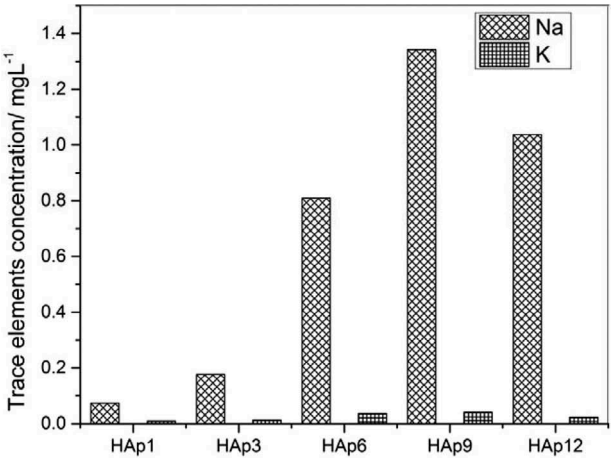

Figure 5. Influence of stirring time on trace element concentration: HAp1, HAp3, HAp6, HAp9, HAp12 are powders prepared at varying stirring times; 1 hr, 3 hrs, 6 hrs, 9 hrs, and 12 hrs, respectively.

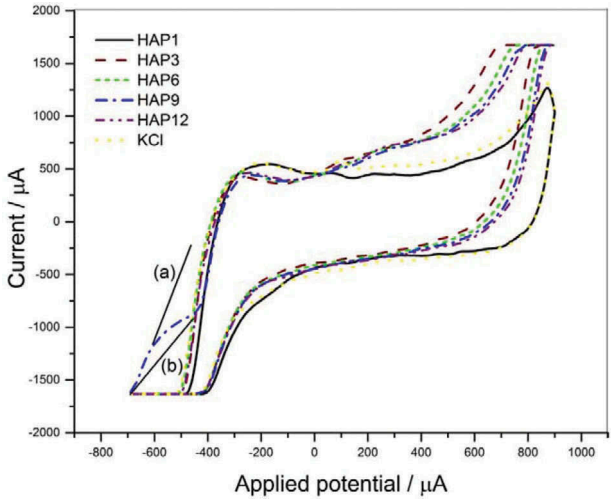

Figure 6. Cyclic voltammogram of samples. Samples were mixed with 1 M KCl to activate ions. (a) and (b) indicates a transition from reversible electron transfer to an irreversible electron transfer, respectively.

HAp1 but when the stirring time was increased to 9 hrs, the concentration increased and then decreased at 12 hrs (See HAp9 and HAp12 in Figure 5). A similar trend occurred for K.

The variation of the trace element concentration at a constant temperature with stirring times is suspected to be due to substitution. The ions are in the lattice sites of the crystalline structure and diffuse to the surface by prolonged stirring at a constant temperature. Ion substitution has been reported [36] in Hap, where Pb and Na ions replace Ca ions.

3.4. CV

Figure 6 shows the cyclic voltammogram of HAp powders mixed with 1M KCl solution. A potential was applied to the mixture on the working electrode to transfer electrons to the mixture (cathodic reaction) thus reducing the mixture. A peak current was recorded and the potential was lowered to release electrons from the mixture to the electrode (anodic reaction) for oxidation to occur.

A reversing peak obtained for all the HAp mixtures indicate a complete reversible electron transfer reaction. Relatively, high peak currents were recorded for all the mixtures except for HAp1. This observation could be attributed to the fact that trace elements that diffused to the surface of the working electrode were few, as revealed by AAS. Since the concentration of trace elements in the HAp samples increased as the stirring time increased, it is suspected that substantial amounts of trace elements in HAp1 may have been locked up in the lattice sites. Hence, ions were inaccessible to the electrode surface for electron transfer.

The cyclic voltammogram of HAp9 shows a transition from reversible electron transfer to an irreversible electron transfer (indicated as (a) and (b), respectively, in Figure 6). This is suggestive of an initial high concentration of trace elements on the electrode surface available for electron transfer. As the applied potential increased, it is suspected that the concentration at the electrode surface diminished thus causing mass diffusion rate (diffusion of ions from the bulk solution to the electrode surface) to be higher than electron transfer rate and this may have accounted for the transition from reversibility to irreversibility.

3.5. Fluoride removal and pH changes

Figure 7 and Figure 8 show the concentrations of fluoride and pH of the supernatant, respectively after the HAp samples were immersed in aqueous fluoride solution of concentration, 20 mgL^{-1}.

It is observed that the CO_3^{2-} and Na^+ substitution as confirmed by XRD and AAS, respectively, in HAp1 is Type B and Type *AB* carbonated apatite substitution as reported [13]. In Type B, CO_3^{2-} and Na^+ replaces PO_4^{3-} and Ca^{2+}, respectively, whilst in Type *AB*, both PO_4^{3-} and OH^- are substituted by two

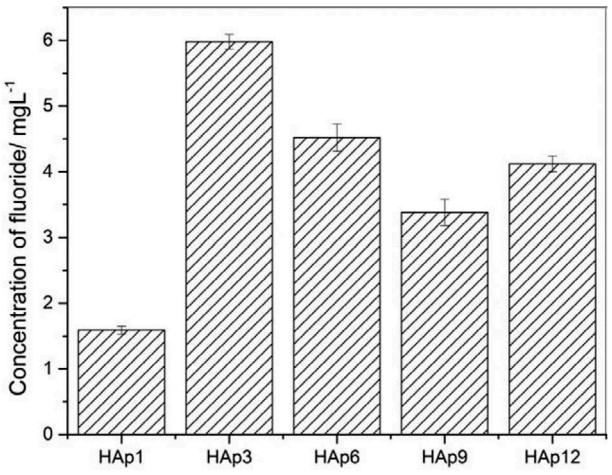

Figure 7. Concentration of fluoride in supernatant after treatment with HAp powders: HAp1, HAp3, HAp6, HAp9, and HAp12 are powders prepared at varying stirring times; 1 hr, 3 hrs, 6 hrs, 9 hrs, and 12 hrs, respectively. The initial concentration of fluoride was 20 mgL^{-1}.

CO_3^{2-} groups. The substitution resulted in a net charge of + 1 (see Figure 9(b)). The structure model in Figure 9(b) suggests that fluoride removal from the solution was through ionic bonding between calcium ions and fluoride ions. This adsorption mechanism did not affect the pH conditions of the solution much. However, high pH values were recorded for the supernatants of HAp3, HAp6, HAp9, and HAp12. The high pH values were due to ion exchange between hydroxyl groups of HAp (see the model in Figure 9(a)) and fluoride ions.

The substitution also favoured the fluoride removal capability in HAp1 than HAp3, HAp6, HAp9, and HAp12 (see Figure 7). This was because as more hydroxyl groups are released from the material into solution. The solution becomes more basic and causes the hydroxyl groups of the HAp to become deprotonated, making it more negative and thus repelling fluoride ions in solution [37]. Further

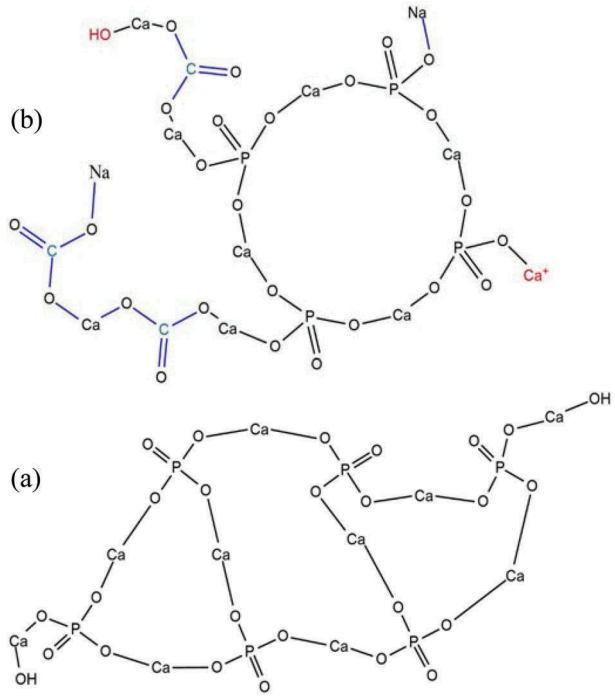

Figure 9. Chemical structures of (a) Pure HAp unit cell (b) HAp1 unit cell: modified HAp showing substitution; Type B and Type *AB* where Na^+ replaces Ca^{2+}, CO_3^{2-} and CO_3^{2-} replaces OH^-, PO_4^{3-}, respectively. The structures were drawn using ChemDraw Pro 12.0.

removal is suspected to be facilitated through electrostatic interactions by Na and K ions occupying the interstitial sites of HAp as revealed at the surface of the HAp by AAS. The HAp with the highest surface ions had the highest fluoride removal. The fluoride removal did not depend on the crystallite size.

4. Conclusion

HAp powders were prepared from AA snail shells and phosphate-containing solution. Stirring time was varied at a constant temperature to control the crystallite size

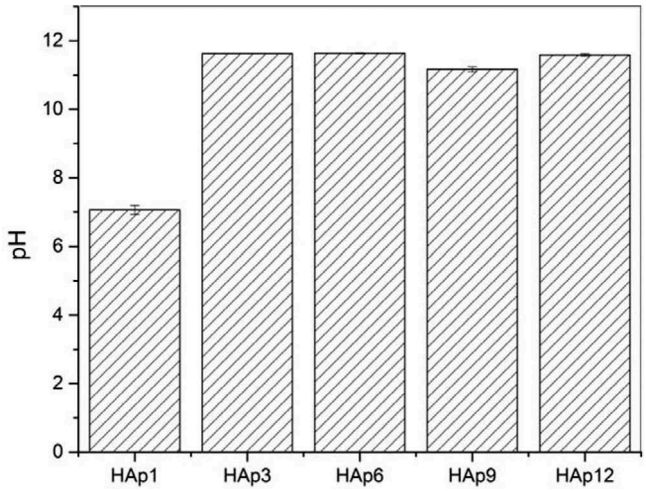

Figure 8. pH changes of supernatant after treatment with HAp powders: HAp1, HAp3, HAp6, HAp9, and HAp12 are powders prepared at varying stirring times; 1 hr, 3 hrs, 6 hrs, 9 hrs, and 12 hrs, respectively. The initial pH of solution was 6.80 ± 021.

and trace element concentration at the surface. HAp samples prepared following 1 hr of stirring (HAp1) were able to reduce fluoride concentration of 20.00 to 1.59 ± 0.06 mgL^{-1} with minimal changes in pH conditions. XRD and AAS revealed CO_3^{2-} and Na^+ substitution, respectively and these results were confirmed by FT-IR from the functional groups present and cyclic voltammograms, respectively. The substitution is suspected to be Type B where CO_3^{2-} and Na^+ replace PO_4^{3-} and Ca^{2+}, respectively, and mixed Type *AB* where CO_3^{2-} replaces both PO_4^{3-} and OH^- of HAp. The fluoride removal by HAp1 was suspected to be through ionic bonding interaction between calcium and fluoride ions. HAp1 is a potential cost-effective fluoride removal material and should be exploited. Further studies should include the adsorption conditions, retention, and regeneration time for water purification.

Acknowledgements

Authors acknowledge the support from West African Centre for Cell Biology for Infectious Pathogens for the use of lab space and equipment.

Disclosure statement

No potential conflict of interest was reported by the authors.

ORCID

Bernard Owusu Asimeng http://orcid.org/0000-0002-4847-450X
Elsie Effah Kaufmann http://orcid.org/0000-0001-7675-4333
Claude Fiifi Hayford http://orcid.org/0000-0002-6206-1074
Prince Atsu Anani http://orcid.org/0000-0002-8512-2634
Obed Korshie Dzikunu http://orcid.org/0000-0002-1122-0629

References

[1] Ben-Nissan B. Nanoceramics in biomedical applications. MRS Bull. 2004;29:28–32.
[2] Zhang X, Vecchio KS. Conversion of natural marine skeletons as scaffolds for bone tissue engineering. *Front. Mater. Sci.* 2013;7:103–117.
[3] Cegla RNR, Macha IJ, Ben-Nissan B, et al. Comparative study of conversion of coral with ammonium dihydrogen phosphate and orthophosphoric acid to produce calcium phosphates. *J. Aust. Ceram. Soc.* 2014;50:154–161.
[4] Pazarlioglu SS, Gokce H, Ozyegin S, et al. Effect of sintering on the microstructural and mechanical properties of meleagris gallopova hydroxyapatite. *Biomed. Mater. Eng.* 2014;24:1751–1769.
[5] Treccani L, Yvonne Klein T, Meder F, et al. Functionalized ceramics for biomedical, biotechnological and environmental applications. Acta Biomater. 2013;9:7115–7150.
[6] Ruiz-Hitzky E, Aranda P, Darder M, et al. Hybrid materials based on clays for environmental and biomedical applications. *J. Mater. Chem.* 2010;20:9306.
[7] Jiang SD, Yao QZ, Zhou GT, et al. Fabrication of hydroxyapatite hierarchical hollow microspheres and potential application in water treatment. *J. Phys. Chem. C.* 2012;116:4484–4492.
[8] Gautam RK, Chattopadhyaya MC. Technologies for water cleanup. New Trends: In Nanomaterials for Wastewater Treatment, edited by McCombs K. *Elsevier*. 2016;19:32.
[9] Kanno CM, Sanders RL, Flynn SM, et al. Novel apatite-based sorbent for defluoridation: synthesis and sorption characteristics of nano-micro-crystalline hydroxyapatite-coated-limestone. *Environ. Sci. Technol.* 2014;48:5798–5807.
[10] Terasaka S, Kamitakahara M, Yokoi T, et al. Ability of hydroxyapatite synthesized from waste oyster shells to remove fluoride ions. *Mater. Trans.* 2015;56:1509–1512.
[11] Chen L, Zhang KS, He JY, et al. Enhanced fluoride removal from water by sulfate-doped hydroxyapatite hierarchical hollow microspheres. *Chem. Eng. J.* 2016;285:616–624.
[12] Sani T, Gómez-Hortigüela L, Pérez-Pariente J, et al. Defluoridation performance of nano-hydroxyapatite/stilbite composite compared with bone char. *Sep. Purif. Technol.* 2016;157:241–248.
[13] Ren F, Lu X, Leng Y. Ab initio simulation on the crystal structure and elastic properties of carbonated apatite. *J. Mech. Behav. Biomed. Mater.* 2013;26:59–67.
[14] Li Y, Li D, Weng W. Preparation of nano carbonate-substituted hydroxyapatite from an amorphous precursor. *Int. J. Appl. Ceram. Technol.* 2008;5:442–448.
[15] Bonfield W, Gibson IR. Novel synthesis and characterization of an AB-type carbonate-substituted hydroxyapatite. *J. Biomed. Mater. Res.* 2002;59:697–708.
[16] Kumar GS, Sathish L, Govindan R, et al. Utilization of snail shells to synthesise hydroxyapatite nanorods for orthopedic applications. RSC Adv. 2015;5:39544–39548.
[17] Singh A, Purohit KM. Chemical Synthesis. Characterization and bioactivity evaluation of hydroxyapatite prepared from garden snail (Helix aspersa). *J. Bioprocess. Biotech.* 2011;1:2–5.
[18] Adak MD, Purohit KM. Synthesis of nano-crystalline hydroxyapatite from dead snail shells for biological implantation. *Trends Biomater. Artif. Organs.* 2011;2011(25):101–106.
[19] Essabir H, Bensalah MO, Rodrigue D, et al. A comparison between bio- and mineral calcium carbonate on the properties of polypropylene composites. *Constr. Build. Mater.* 2017;134:549–555.
[20] Eneji IS, Wuana RA, Akpan UJ. Trace metals levels in African giant land snails (Achatina achatina) from selected local government areas in Akwa Ibom State. Nigeria. 2016;1–9. DOI:10.4236/oalib.1102244
[21] Towett EK, Shepherd KD, Tondoh JE, et al. Total elemental composition of soils in Sub-Saharan Africa and relationship with soil forming factors. Geoderma Reg. 2015;5:157–168.
[22] Khandelwal H, Synthesis PS. Characterization of hydroxyapatite powder by eggshell. *J. Miner. Mater. Charact. Eng.* 2016;4:119–126.
[23] Raj MS, Arkin VH, Jagannath M. Nanocomposites based on polymer and hydroxyapatite for drug

delivery application. Indian J. of Sci. Technol. 2013;6:4653–4658.
[24] Sobczak A, Kowalski Z, Wzorek Z. Preparation of hydroxyapatite from animal bones. *Acta Bioeng. Biomech*. 2009;11:23–28.
[25] Nayak A, Laha B, Sen K. Development of hydroxyapatite-ciprofloxacin bone-implants using quality by design. Acta Pharm. 2011;61:25–36.
[26] Akram M, Ahmed R, Shakir I, et al. Extracting hydroxyapatite and its precursors from natural resources. *J. Mater. Sci*. 2014;49:1461–1475.
[27] Barroug A, Glimcher MJ. Hydroxyapatite crystals as a local delivery system for cisplatin: adsorption and release of cisplatin in vitro. *J. Orthop. Res*. 2002;20:274–280.
[28] Ruiz-Agudo E, C V P, Putnis A. Coupled dissolution and precipitation at mineral-fluid interfaces. *Chem. Geol*. 2014;383:132–146.
[29] Fleet ME. The carbonate ion in hydroxyapatite: recent X-ray and infrared results. Front. Biosci. Elite Ed;. 2013;5:643–652.
[30] Ibrahim DM, Mostafa AA, Korowash SI. Chemical characterization of some substituted hydroxyapatites. *Chem. Cent. J*. 2011;5:74.
[31] Murugan R, Ramakrishna S. Development of cell-responsive nanophase hydroxyapatite for tissue engineering. *Am. J. Biochem. Biotechnol*. 2007;3:118–124.
[32] Vahur S, Teearu A, Peets P, et al. ATR-FT-IR spectral collection of conservation materials in the extended region of 4000-80 cm^{-1}. *Anal. Bioanal. Chem*. 2016;408:3373–3379.
[33] Mondal S, De Anda Reyes ME, Pal U. Plasmon induced enhanced photocatalytic activity of gold loaded hydroxyapatite nanoparticles for methylene blue degradation under visible light. RSC Adv. 2017;7:8633–8645.
[34] Nedunchezhian G, Benny Anburaj D, Sembian Ruso J, et al. Fabrication of hydroxyapatite nanorods from land- snail shell (Helix pomatia) assisted by microwave irradiation. In: Indo – asian J. Multi. Res. 2015;1:345–354.
[35] Linstrom PJPJ, Mallard WGG NIST. Chemistry webbook; NIST standard reference database No. 69. *NIST Chem. Webb*. 2001;20899. DOI:10.18434/T4D303
[36] Dong L, Zhu Z, Qiu Y, et al. Removal of lead from aqueous solution by hydroxyapatite/magnetite composite adsorbent. *Chem. Eng. J*. 2010;165:827–834.
[37] Samant A, Nayak B, Misra PK. Journal of Environmental Chemical Engineering Kinetics and mechanistic interpretation of fluoride removal by nanocrystalline hydroxyapatite derived from Limacine artica shells. *J. Environ. Chem. Eng*. 2017;5:5429–5438.